Theoretical Studies on the Magnetic Bistability of Dinickel Complex Tuned by Azide

Jiangyu Bian, Yingfei Chang, and Jingping Zhang*

Faculty of Chemistry, Northeast Normal University, Changchun, 130024, China

Received: November 22, 2007; In Final Form: January 24, 2008

The magnetic-structural correlation in magnetic switchable dinickel(II) complex $[LNi_2(N_3)_3]$ (L^- is a pyrazolate-based compartmental ligand) has been investigated on the basis of various unrestricted density functional theory (UDFT) combined with the broken symmetry (BS) approach. The calculated exchange coupling constants were in good agreement with experimental result by using the PBE0 method with LANL2DZ basis set. The antiferromagnetic interaction between the Ni(II) ions is mainly due to the large energy difference of the singly occupied molecular orbitals (SOMOs), and the p orbital overlap for nitrogen atoms on azido and the pyrazolate bridge groups. The analysis of the spin density distribution reveals that both the spin polarization and spin delocalization contribute to the antiferromagnetic interaction. Furthermore, the bistable magnetic behavior for this system (strong antiferromagnetic interaction in low-temperature phase and the week antiferromagnetic in high-temperature phase) results from the change of the Ni−NNN−Ni dihedral angle (τ) in $\mu_{1,3}$-N_3. The increase of τ is the key role in decreasing the SOMOs energy difference and weakening the antiferromagnetic interaction. Therefore, the abrupt modulation of the magnitude of M−NNN−M dihedral angle τ in the binuclear-azide complex by external perturbations provides new possibilities for the design of molecular magnetic switching devices.

1. Introduction

Bistable materials, which can persist in two relatively stable states, each with different physical properties (optical, electrical, magnetic, and/or mechanical properties), have great potential in next-generation sensor, switching, and/or actuator devices.[1,2] Especially, the property of thermal magnetic hysteresis changed abruptly and rapidly around room temperature is particularly rare for molecule-based materials.[3,4] One of the most spectacular examples of molecular bistability is the spin-crossover phenomenon. It was first observed in 1931,[5,6] and has been investigated extensively since the mid-1970s.[7,8] In 1999, the discovery of the room-temperature magnetic bistability in an organic radical, 1,3,5-trithia-2,4,6-triazapentalenyl by Fujita et al. owing to intermolecular dimerization, opened a new branch in this field.[9] This important finding suggests low dimension magnetic system to be potential molecular bistable system. In particular, the alkyl-substituted spirobiphenalenyl radicals display that optical, electrical, and magnetic properties can be simultaneously switched.[10,11] Recently, a series of compartmental pyrazolate-based ligands nickel(II)-azide magnetic complexes have been studied by Leibeling et al.[12] Peculiarly, the dinickel(II)−$\mu_{1,3}$-azide complex $[LNi_2(N_3)_3]$ shows the magnetic bistable property, i.e., strong antiferromagnetic interaction in low-temperature phase and the week antiferromagnetic in high-temperature phase which is tuned by $\mu_{1,3}$-azido ligand.[12a] They proposed that the cause of the unusual magnetic properties is the change in Ni−NNN−Ni torsion. One of the ligands in this bistable complex, pyrazolate-based compartmental ligand L^- (Figure 1) has been proven suitable as dinucleating scaffolds for the synthesis of preorganized azido−nickel(II) complexes that can serve as modules for the assembly of oligonuclear species or 1D extended chain compounds.[13] While another ligand azido anion is known as a versatile ligand that can bind to transition metal atoms with different coordination modes, thus allowing for the assembly of binuclear complexes with range of magnetic behavior. Most commonly, the azide ion can adopt two possible bridging modes: end-to-end (EE, $\mu_{1,3}$-) associated with antiferromagnetic (AF) coupling, and end-on (EO, $\mu_{1,1}$-) related with ferromagnetic exchange. In this case, the M−N−M angle in $\mu_{1,1}$-N_3, the M−N−N angle, and the M−NNN−M dihedral angle in $\mu_{1,3}$-N_3 are the key factors in tuning the magnetic interaction.[14]

In the dinickel(II)-azide magnetic bistable complex, the azido ligand acts as an on/off switch through the different M−NNN−M dihedral angle τ and similar M−N−N angle. Although this task can be addressed from the theoretical standpoint, a few computational works relating to this type of materials can be found in the literature.[15,16] To the best of our knowledge, no theoretical investigation for this complex has been reported so far to explain the magnetic bistable property. In this work, we attempt to explore the origin of the magnetic switching for the dinickel(II)-azide magnetic bistable complex $[LNi_2(N_3)_3]$, and the role of $\mu_{1,3}$-N_3 bridging in magnetic transition.

2. Theoretical Background

The interaction between two magnetic centers can be described with the Heisenberg−Dirac van Vleck Hamiltonian model:[17,18]

$$\hat{H} = -2J_{ab}\vec{S}_a\vec{S}_b \tag{1}$$

Here J_{ab} is the magnetic coupling between the unpaired electrons in sites *a* and *b*. Positive value of the coupling constant J_{ab} indicates ferromagnetic character, and negative value of J_{ab} shows antiferromagnetic behavior.

The broken-symmetry (BS) DFT strategy has been applied as a practical tool for the study of magnetic interactions on rather

* Corresponding author. Fax: +8643185684937. E-mail: zhangjingping66@yahoo.com.cn.

10.1021/jp711121z CCC: $40.75
Published on Web 03/07/2008

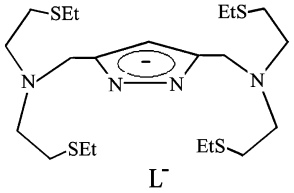

Figure 1. Pyrazolate-based compartmental ligand L^-.

large systems with reasonable accuracy and partial considerations of the electron correlation effects.[19] Assuming the so-called "weak bonding" regime, Ginzberg,[20] Noodleman,[21] and Davidson[22] (GND) evaluate the magnetic coupling within broken symmetry framework by

$$J_{ab}^{(1)} = \frac{^{LS}E(X) - {}^{HS}E(X)}{{S_{max}}^2} \quad (2)$$

However, in the strong overlap region, GND, Bencini,[23] Ruiz[24] and others suggested that the following expression might give more reasonable solutions.

$$J_{ab}^{(2)} = \frac{^{LS}E(X) - {}^{HS}E(X)}{S_{max}(S_{max}+1)} \quad (3)$$

The approximate spin projection procedure involving the expectation value of the total spin angular momentum $\langle S^2 \rangle$ has also been introduced to evaluate J_{ab} values.[25]

$$J_{ab}^{(3)} = \frac{^{LS}E(X) - {}^{HS}E(X)}{^{HS}\langle S^2 \rangle - {}^{LS}\langle S^2 \rangle} \quad (4)$$

where $^{Y}E(X)$ and $^{Y}\langle S^2 \rangle$ (X) denote, total energy and total spin angular momentum for the spin state Y by the method X (=UHF, UDFT, etc.), respectively. The third scheme $J_{ab}^{(3)}$ is close to $J_{ab}^{(1)}$ by GND if $^{HS}\langle S^2 \rangle \approx S_{max}(S_{max}+1)$ and $^{LS}\langle S^2 \rangle \approx S_{max}$, where S_{max} is the spin size for the high spin state. $J_{ab}^{(3)}$ becomes equivalent to $J_{ab}^{(2)}$ in the strong overlap region, where $^{LS}\langle S^2 \rangle \approx 0$.[26]

3. Calculation Structures and Methods

3.1. Description of the Calculated Models. Four X-ray crystallography structures of $[LNi_2(N_3)_3]$ at 133, 195, 223, and 253 K were obtained experimentally; i.e., two structures at low temperature are denoted by 1-LT (133 K) and 2-LT (195 K), and two structures at high temperature are named by 1-HT (223 K) and 2-HT (253 K). A major change of the Ni−NNN−Ni dihedral angle τ (the dihedral angle between the mean planes M−N−N−N and N−N−N−M′) in $\mu_{1,3}$-N_3 is observed between 2-LT and 1-HT, while no significant variations for the dihedral angles between 1-LT and 2-LT or between 1-HT and 2-HT are found.[12a] Therefore, only the structures in 1-LT and 2-HT are shown in Figure 2. It is experimentally well-known that the measured exchange coupling constants are affected largely by small deviations in bond angles and bond lengths of the molecule, thus the optimized geometry structure in gas-phase usually cannot reproduce well the experimental results.[27] On the other hand, because quantum chemical calculations cannot treat temperature explicitly, in current calculations, the molecular structures at different temperature for the complex are taken directly from the X-ray crystallography structure.[12a]

3.2. Calculation Methods. Combined with the broken-symmetry approach, several DFT functionals such as the local spin density approach (SVWN), the generalized gradient approximations (BP86, BPW91, BLYP, and PBE), and the hybrid functional methods (B3P86, B3LYP, B3PW91, and PBE0) with the LANL2DZ basis set were employed to evaluate the magnetic coupling constant J_{ab}. On the basis of the selected functional (PBE0), various basis sets such as LANL2DZ, 6-31G, TZVP, and Ahlrichs PVDZ were used to examine the basis set dependence of the J_{ab} values. All computations were carried out with the Gaussian 03 suite of programs.[28]

4. Results and Discussion

4.1. Magnetic Coupling Constant J_{ab}. All the J_{ab} values for 1-LT, 2-LT, 1-HT and 2-HT with various approaches are listed in Table 1. The calculated results indicate that the J_{ab} values are computational methods dependent with the LANL2DZ basis set, and the $|J_{ab}^{(3)}|$ value for the four structures by each method is slightly smaller than the $|J_{ab}^{(1)}|$ value, because of the non-negligible orbital overlap between the magnetic orbitals. As the previous report claimed that J_{ab} value obtained by the approximate spin projection procedure reproduces the characteristic feature of J_{ab} in the whole region, while the other two strategies only work in weak or strong overlap regions,[25] only the $J_{ab}^{(3)}$ values obtained from eq 4 are thus employed in the following discussion.

All calculated $J_{ab}^{(3)}$ values are in a qualitative agreement with the observed antiferromagnetic interaction (Table 1). For 1-LT, the $J_{ab}^{(3)}$ values computed with the UB3PW91, UB3P86, and UPBE0 are −72.12, −71.72, and −101.10 cm^{-1}, respectively, and agree well with the observed experimental value $-(81 \pm 1.5)$ cm^{-1}. The magnitude of the calculated $J_{ab}^{(3)}$ values increases in the order UB3P86 < UB3PW91 < UPBE0 < UB3LYP < UPBE < UBLYP < UBPW91 < UBP86 < USVWN. The $J_{ab}^{(3)}$ values for 1-HT computed with the UB3PW91 (−44.96 cm^{-1}), UB3LYP (−45.19 cm^{-1}), and UPBE0 (−21.23 cm^{-1}) agree with the experimental value $-(24 \pm 1.0)$ cm^{-1}, especially for UPBE0, while much more negative $J_{ab}^{(3)}$ values are derived with the remaining functionals. However, for 2-LT and 2-HT, only the UPBE0 calculated $J_{ab}^{(3)}$ values (−99.87 cm^{-1} for 2-LT and −19.51 cm^{-1} for 2-HT) are in good agreement with the experimental data. Judging by the $J_{ab}^{(3)}$ values in Table 1, it is clearly shown that the PBE0 can provide more reasonable results in the treatment of the magnetic systems with enough accuracy and reliability, as reported in our previous work[29] and by another group.[30] To examine the basis set dependence of the $J_{ab}^{(3)}$ values, we performed PBE0 calculations with various basis sets such as LANL2DZ, 6-31G, TZVP, and Ahlrichs PVDZ (Table 2). The results suggest that the PBE0 calculation for $J_{ab}^{(3)}$ values are basis sets independent for the basis sets used. Thus, we utilize the UPBE0/LANL2DZ results to evaluate the magnetic interactions and Ni−NNN−Ni dihedral angle τ effect on $J_{ab}^{(3)}$ values in dinickel(II) complex $[LNi_2(N_3)_3]$. It is worth noting that the $J_{ab}^{(3)}$ values are similar for 1-LT (133 K) and 2-LT (195 K) or 1-HT (223 K) and 2-HT (253 K); this feature is ascribed to their similar dihedral angles. Therefore, in the following section we will select the molecule structures 1-LT (133 K) and 2-HT (253 K) to explore the nature of the transition between high- and low-temperature phases and the effect of the Ni−NNN−Ni dihedral angle τ on their magnetic behaviors.

4.2. Molecular Magnetic Orbitals. In molecular magnetism, the orbitals which are located on the local spin centers are called local magnetic orbitals, while the single-occupied molecular orbitals (SOMOs) in the high spin state are regarded as

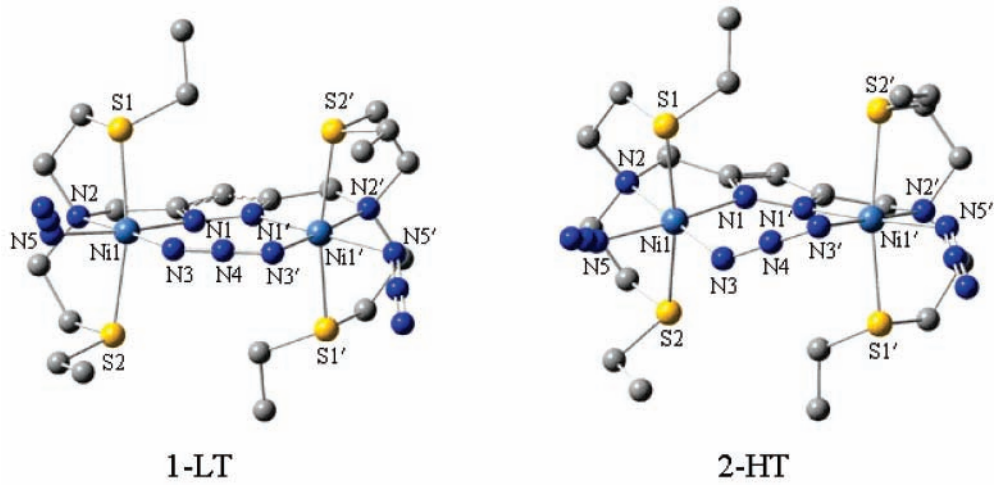

Figure 2. Structures of $[LNi_2(N_3)_3]$ at 133 K (1-LT) and 253 K (2-HT), hydrogen atoms are not shown.

TABLE 1: Total Energies and Total Spin Angular Momentum for the Singlet and Quintet States and the J_{ab} Values for 1-LT, 2-LT, 1-HT, and 2-HT Obtained by Several DFT Functional Calculations with LANL2DZ Basis Set[a]

complex	method	E_{BS}	E_{QS}	$J_{ab}^{(1)}$	$J_{ab}^{(2)}$	$\langle S^2\rangle_{BS}$	$\langle S^2\rangle_{QS}$	$J_{ab}^{(3)}$	exp
1-LT	PBE0	−1913.083597	−1913.081751	−101.29	−67.53	2.007413	6.015154	−101.10	−(81 ± 1.5)
	B3PW91	−1914.574807	−1914.573488	−72.42	−48.28	1.997546	6.014081	−72.12	
	B3LYP[b]	−1914.963345	−1914.961235	−115.77	−77.18	1.998891	6.014206	−115.33	
	B3P86	−1921.058876	−1921.057563	−72.04	−48.02	1.996278	6.013775	−71.72	
	BPW91	−1915.063432	−1915.058947	−246.10	−164.06	1.891225	6.008373	−239.09	
	BP86	−1915.304818	−1915.299212	−307.60	−205.07	1.881618	6.007966	−298.19	
	BLYP	−1914.076759	−1914.072896	−211.94	−141.29	1.88958	6.008424	−205.82	
	PBE	−1913.105151	−1913.101779	−185.05	−123.37	1.88109	6.008763	−179.33	
	SVWN	−1907.138173	−1907.130557	−417.91	−278.60	1.716605	6.010494	−389.30	
2-LT	PBE0	−1913.075939	−1913.074115	−100.07	−66.72	2.006611	6.014994	−99.87	−(81 ± 1.5)
	B3PW91	−1914.567078	−1914.564865	−121.42	−80.95	1.997134	6.013788	−120.92	
	B3LYP	−1914.95425	−1914.951745	−137.41	−91.61	1.99732	6.013765	−136.84	
	B3P86	−1921.051795	−1921.049624	−119.12	−79.41	1.9976	6.013735	−118.64	
	BPW91	−1915.053033	−1915.049128	−214.26	−142.84	1.895044	6.008371	−208.36	
	BP86	−1915.294557	−1915.28937	−284.60	−189.73	1.886078	6.008003	−276.18	
	BLYP	−1914.066445	−1914.06214	−236.19	−157.46	1.89407	6.008366	−229.63	
	PBE	−1913.095964	−1913.090993	−272.71	−181.81	1.883281	6.008427	−264.43	
	SVWN	−1907.128855	−1907.121597	−398.19	−265.46	1.711166	6.010463	−370.48	
1-HT	PBE0	−1912.968195	−1912.967808	−21.26	−14.17	2.012454	6.018035	−21.23	−(24 ± 1.0)
	B3PW91	−1914.458924	−1914.458103	−45.05	−30.04	2.007761	6.016198	−44.96	
	B3LYP[b]	−1914.843786	−1914.842961	−45.29	−30.19	2.00736	6.016062	−45.19	
	B3P86	−1920.943653	−1920.942671	−53.89	−35.93	2.001665	6.016601	−53.69	
	BPW91	−1914.937077	−1914.934967	−115.78	−77.19	1.951168	6.009414	−114.12	
	BP86	−1915.176511	−1915.174353	−118.39	−78.93	1.946435	6.009	−116.57	
	BLYP	−1913.946636	−1913.944906	−94.94	−63.29	1.951923	6.009449	−93.59	
	PBE	−1912.979266	−1912.977651	−88.59	−59.06	1.949465	6.009682	−87.27	
	SVWN	−1907.018456	−1907.015198	−178.78	−119.18	1.857286	6.011325	−172.14	
2-HT	PBE0	−1912.861697	−1912.86134	−19.56	−13.04	2.009733	6.018132	−19.51	−(24 ± 1.0)
	B3PW91	−1914.351973	−1914.351015	−52.54	−35.03	2.005597	6.016599	−52.40	
	B3LYP[b]	−1914.736458	−1914.735568	−48.81	−32.54	2.006537	6.015635	−48.69	
	B3P86	−1920.837716	−1920.836586	−62.01	−41.34	2.006748	6.016286	−61.86	
	BPW91	−1914.826369	−1914.824509	−102.07	−68.05	1.945554	6.009314	−100.47	
	BP86	−1915.063299	−1915.061747	−85.18	−56.79	1.910116	6.008859	−83.13	
	BLYP	−1913.834287	−1913.832767	−83.39	−55.60	1.946166	6.009249	−82.10	
	PBE	−1912.867664	−1912.865809	−101.76	−67.84	1.946554	6.009591	−100.18	
	SVWN	−1906.909383	−1906.906408	−163.25	−108.83	1.855134	6.010997	−157.13	

[a] Total energies are in au, J_{ab} are shown in cm^{-1}. $J_{ab}^{(1)}$, $J_{ab}^{(2)}$ and $J_{ab}^{(3)}$ correspond to eqs 2, 3 and 4, respectively. [b] The STABLE = OPT option is used for the BS calculation.

molecular magnetic orbitals; generally, the latter determine the magnetic behaviors of the molecular systems. In the $[LNi_2(N_3)_3]$ complex considered, the coupling interaction between two spin carriers Ni(II) is the super-exchange type of magnetic exchange through the azido bridge and/or the pyrazolate nitrogen atoms. The SOMOs in the quintet states for 1-LT and 2-HT and their corresponding energies at the ROPBE0/LANL2DZ level are given in Figure 3. From left to right, the four SOMOs are HOMO-3, HOMO-2, HOMO-1 and HOMO, respectively.

On the basis of the Hoffmann theory,[31] the relationship between the magnetic orbitals and the J_{ab} values can be qualitatively understood by analyzing the molecular orbitals. From Figure 3 we can see that the Ni(II) magnetic orbitals are attributed mainly to the d orbitals, nitrogen atoms from both the azido groups and the pyrazolate contribute to the magnetic orbitals as well. For 1-LT or 2-HT, the HOMO and HOMO-3 form from Ni(II)-$d_{x^2-y^2}$-like orbitals and π-orbitals of the azido and the pyrazolate nitrogen atoms, and the HOMO-1 and

TABLE 2: Total Energies and Total Spin Angular Momentum for the Singlet and Quintet States, and the J_{ab} Values for 1-LT and 2-HT Obtained by UPBE0 with Several Basis Sets[a]

complex	basis set	E_{BS}	E_{QS}	$J_{ab}^{(1)}$	$J_{ab}^{(2)}$	$\langle S^2\rangle_{BS}$	$\langle S^2\rangle_{QS}$	$J_{ab}^{(3)}$	exp
1-LT	LANL2DZ	−1913.083597	−1913.081751	−101.29	−67.53	2.007413	6.015154	−101.10	−(81 ± 1.5)
	6-31G	−6141.79968	−6141.797845	−100.69	−67.13	2.007331	6.011158	−100.59	
	TZVP	−6143.470578	−6143.469265	−72.03	−48.02	2.007 94	6.015854	−71.88	
	Ahlrichs PVTZ	−6140.893309	−6140.89151	−98.73	−65.82	2.005 97	6.012884	−98.55	
2-HT	LANL2DZ	−1912.861697	−1912.86134	−19.56	−13.04	2.009733	6.018132	−19.51	−(24 ± 1.0)
	6-31G	−6141.584033	−6141.583882	−8.26	−5.51	2.009124	6.014133	−8.25	
	TZVP	−6143.27963	−6143.278855	−42.53	−28.35	2.011953	6.018146	−42.46	
	Ahlrichs PVTZ	−6140.68764	−6140.686904	−40.41	−26.94	2.009956	6.015453	−40.36	

[a] Total energies are in a.u., J_{ab} are shown in cm^{-1}. $J_{ab}^{(1)}$, $J_{ab}^{(2)}$ and $J_{ab}^{(3)}$ correspond to eqs 2, 3, and 4, respectively.

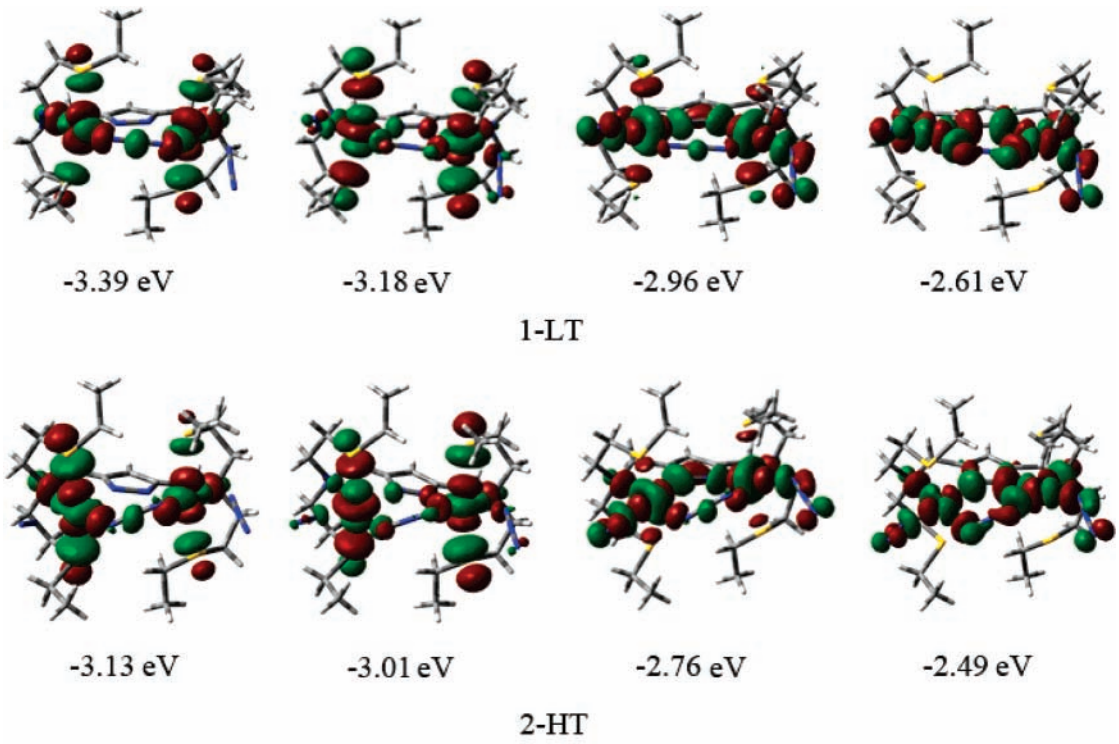

Figure 3. SOMOs for 1-LT and 2-HT in the quintet states and their corresponding energies at the ROPBE0/LANL2DZ level. From left to right, the four SOMOs are HOMO-3, HOMO-2, HOMO-1, and HOMO, respectively.

HOMO-2 are formed from Ni(II)-d_{z^2}-like orbitals and π-orbitals of the azido and the pyrazolate nitrogen atoms. The distribution pattern of the SOMOs suggests that two path ways for the exchange interaction between the Ni(II) ions are the nitrogen atoms N1, N1′ of pyrazolate and the $\mu_{1,3}$-N_3 as bridges. For 1-LT or 2-HT, there is p orbital overlap between N1 and N1′ of pyrazolate in HOMO-1, and between N3′ and N4 of azido in HOMO, respectively. Therefore, two path ways all contribute to the antiferromagnetic coupling.

According to our DFT calculations, the energy splitting of SOMOs, i.e., the energy deference between HOMO-3 and HOMO of the 1-LT and 2-HT are 0.78 and 0.64 eV, respectively. The large energy splittings of SOMOs in 1-LT and 2-HT are also responsible for their strong antiferromagnetic couplings. Furthermore, the antiferromagnetic component of the 1-LT is stronger than that of the 2-HT due to its larger energy splitting of SOMOs. This result can be explained by the fact that the observed Ni−NNN−Ni dihedral angle in the crystallized complexes is 4.34° for 1-LT and −46.46° for 2-HT, Ni−N1−N1′−Ni dihedral angle is 23.16° for 1-LT and −38.86° for 2-HT. The severe tilting of the azido bridge in 2-HT leads to the decrease of the energy deference between the HOMO-3 and HOMO, corresponding to the weak antiferromagnetic interactions.

TABLE 3: Spin Density Distributions for 1-LT and 2-HT in the Singlet State

	Ni1	N3	N4	N3′	Ni1′	N1	N1′
1-LT	−1.542	0.063	0.000	−0.064	1.540	−0.055	0.055
2-HT	1.542	−0.055	−0.004	0.063	−1.551	0.056	−0.055

4.3. Spin Delocalization and Polarization. As shown previously,[32] the spin densities are not strictly related to real spin populations as in the case of antiferromagnetic solids, but they are useful indices to express the magnitude of spin systems. From the point of view of molecular orbital theory, the spin delocalization can be explained as a transfer of unpaired electron density from the metal to the ligand atoms. While the spin polarization results from the optimization of the electronic exchange and coulomb terms and induces the spin distribution with alternating sign for the successive ligand atoms. Table 3 lists the spin density distributions for 1-LT and 2-HT in the singlet state as obtained by UPBE0 calculations on the basis of Mulliken population analysis. The positive and negative signs indicate α and β spin states, respectively.

For the investigated complex, the spin populations in the BS state (see Table 3) on Ni1 and Ni1′ for 1-LT are −1.542 and +1.540, respectively, demonstrating a part of spin densities delocalization from Ni1 and Ni1′. For the azido bridging ligand,

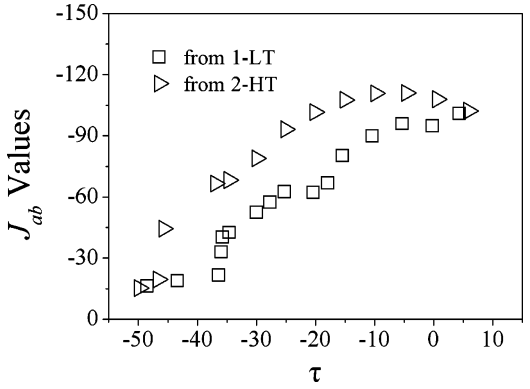

Figure 4. Ni−NNN−Ni dihedral angle (τ) dependence for $J_{ab}^{(3)}$ values.

spin densities on the two terminal atoms N3 and N3′ of the EE azido group are antiparallel, and the signs of spin densities of the Ni1 and N3, N3′ and Ni1′ are alternatively aligned on the whole, suggesting the spin polarization effect in the dinickel-(II) complex $[LNi_2(N_3)_3]$, the spin density on central atom N4 is largely suppressed due to the reversed spin polarization from N3 and N3′, and thus its value approaches zero obviously. As Kahn[33,34] proposed that the HOMO of azido group are occupied by two electrons, this doubly occupied HOMO would be polarized by the magnetic ions that are bridged by the azido group. That means the two electrons with up and down spin in the HOMO will be separated from each other and localized around the two terminal nitrogen atoms of azido group, respectively. The spin densities for Ni1 and N1 or for Ni1′ and N1′ have the same sign, showing the spin delocalization effect, while N1 and N1′ possess different sign. For 2-HT, the spin density distribution pattern is similar to that of 1-LT, only the signs of spin densities are all opposite to those of 1-LT. Therefore, in complex $[LNi_2(N_3)_3]$, both the spin polarization and the spin delocalization effect contribute to the antiferromagnetic interaction in each phase.

4.4. Ni—NNN—Ni Dihedral Angle Dependence of J_{ab} Values. For the two antiferromagnetic coupling paths from azido and pyrazolate of L^-, the conformational effect should play an important role on the exchange interaction. While the steric constrain of L^- limits the effective change of nitrogen atoms on pyrazolate. With the aim to explore in detail the effect of the azido ligand in on/off switch in the dinickel(II)-azide magnetic bistable complex, further study on the relationship between the variation of Ni−NNN−Ni dihedral angle τ and switchable property is of great importance. As the observed τ in the crystallized complexes is 4.34° for 1-LT and −46.46° for 2-HT, respectively, we change τ from 4.34° to −48.52° for 1-LT and from 5.90° to −49.81° for 2-HT to investigate the on/off switch function of the azido bridge ligand, respectively. The rest of the structure is kept in its crystallographic geometry. The trend of the calculated $J_{ab}^{(3)}$ values (Table S1) with variation of the τ is schematically shown in Figure 4.

From Figure 4 we can see that both curves show the same trend. The $J_{ab}^{(3)}$ values for 1-LT or 2-HT are negative in the whole investigated region, suggesting antiferromagnetic interaction. The values of Ni1−N3−N4 angles change from 115.09° to 123.76°. For both 1-LT and 2-HT, the antiferromagnetic interaction is getting weaker with the increasing of τ. For 1-LT, the $J_{ab}^{(3)}$ values change gradually from −101.10 to −16.25 cm^{-1}. The $J_{ab}^{(3)}$ values for 2-HT change rapidly in the beginning (−15.37 to −101.56 cm^{-1}) and then remain around (−101 ± 5) cm^{-1} as τ in the range from −20.09 to 5.90°. The relation

TABLE 4: Changes of Parameters in the Phase Transition from 1-HT to 2-LT

ΔE (kcal/mol)	ΔH (kcal/mol)	ΔG (kcal/mol)	ΔS (cal/mol)
−68.89	−70.75	−65.61	−6.27

of the $J_{ab}^{(3)}$ values (cm^{-1}) with the change of the τ for 1-LT (eq 5) and 2-HT (eq 6) can be expressed as follows:

$$J_{ab}^{(3)} = -98.0678 - 0.7963\tau + 0.0338\tau^2 \quad (5)$$

$$J_{ab}^{(3)} = -108.4987 + 0.6457\tau + 0.0503\tau^2 \quad (6)$$

The correlation coefficients for 1-LT and 2-HT are 0.9654 and 0.9817, respectively.

Therefore, with increasing τ, the transition from a strong antiferromagnetic in low-temperature phase to weak antiferromagnetic high-temperature phase does occur. Thus, the Ni−NNN−Ni dihedral angle is the key factor to tune the magnetic interactions, i.e., the conformational change of the azido bridge results in an abrupt magnetic switch for $[LNi_2(N_3)_3]$ complex. As a consequence, the molecular magnetic switching devices which can be designed by changing the Ni−NNN−Ni dihedral angle τ are expectable.

4.5. The Change of the Energies. During the decrease of the temperature, the energy for 2-HT, 1-HT, 2-LT, and 1-LT is decreasing. From Figure 3 we can see clearly that the SOMOs orbital energy for 1-LT (−3.39, −3.18, −2.96, and −2.61 eV) are lower than those of 2-HT (−3.13, −3.01, −2.76, and −2.49 eV); i.e., the system becomes more stabilized with the temperature decrease. The main changes of the magnetic property in this magnetic bistable complex $[LNi_2(N_3)_3]$ are observed between 1-HT and 2-LT; i.e., the phase transition takes place between 1-HT and 2-LT, which can be qualitatively explained by the changes in the energetic parameters in this process as listed in Table 4. For 1-HT and 2-LT, the difference of the Gibbs free energy ($\Delta G = -65.61$ kcal/mol <0) corresponds to the possibility of the phase transition. For solid-state transition, the difference of entropies ($\Delta S = -6.27$cal/mol) is small enough to be ignored. The calculated result of the enthalpies difference (ΔH) is −70.75 kcal/mol, which shows that the system is radiative ($\Delta H < 0$). And $C_v\Delta T$ (C_v is the constant capacity heat capacity and ΔT is the difference of the temperature) are in the range of 1.36−2.29 kcal/mol, which is much less than ΔH; therefore, the remaining thermal energy ($\Delta H - C_v\Delta T$) can be used to overcome the energy barrier for the phase transition. However, with the temperature increasing, the system can obtain enough energy to across the energy barrier. More detailed analysis about this process is currently under investigation.

5. Conclusion

The broken symmetry (BS) approach within density functional theory (DFT) was applied to investigating magnetic exchange interactions in dinickel(II)-azide magnetic bistable complex. Our calculated exchange coupling constants of complex $[LNi_2(N_3)_3]$ are in good agreement with the experimental phenomena that the material exhibits a transition from strong antiferromagnetic to only weak antiferromagnetic with the temperature increasing. Magnetic exchange mechanism has been presented by SOMO distribution pattern, the energy splitting of SOMOs and Mulliken population analysis. SOMO distribution pattern in two different phases all display the p orbital overlap for nitrogen atoms on azido and the pyrazolate as bridge groups in two interaction paths, corresponding to antiferromagnetic coupling behavior. The spin polarization effect

and the spin delocalization effect compensate with each other and favor for the total antiferromagnetic interaction. The large energy deference for SOMOs is also responsible to the strong antiferromagnetic coupling in low-temperature phase with small Ni−NNN−Ni dihedral angle τ, while the decreasing of energy splitting for SOMOs results in the weak antiferromagnetic coupling in high-temperature phase due to large Ni−NNN−Ni dihedral angle. The detail investigation for exchange coupling constant with the variation of Ni−NNN−Ni dihedral angle suggests clearly that the conformational change of $\mu_{1,3}$-N_3 bridge to be the key factor in the different magnetic exchange interactions found in this bistable system. So the abrupt modulation of the magnitude of Ni−NNN−Ni dihedral angle in the $[LNi_2(N_3)_3]$ complex by external perturbations provides new possibilities for the design of molecular magnetic switching devices.

Acknowledgment. Financial support from the Natural Science Foundation of China (Grant No. 20274006), NCET-06-0321, and NENU-STB-07007 is gratefully acknowledged.

Supporting Information Available: Complete reference for ref 28 and a table of total energies and total spin angular momentum for the singlet and quintet states, and the Ni−NNN−Ni dihedral angles (τ) dependence for $J_{ab}^{(3)}$ of 1-LT and 2-HT at the UPBE0/LANL2DZ level (Table S1). This material is available free of charge via the Internet at http://pubs.acs.org.

References and Notes

(1) Carroll, R. L.; Gorman, C. B. *Angew. Chem., Int. Ed.* **2002**, *41*, 4378.

(2) Bousseksou, A.; Molnár, G.; Matouzenko, G. *Eur. J. Inorg. Chem.* **2004**, *22*, 4353.

(3) (a) Malaun, M.; Reeves, Z. R.; Paul, R. L.; Jeffery, J. C.; McCleverty, J. A.; Ward, M. D.; Asselberghs, I.; Clays, K.; Persoons, A. *Chem. Commun.* **2001**, *1*, 49. (b) Sato, O.; Kawakami, T.; Kimura, M.; Hishiya, S.; Kubo, S.; Einaga, Y. *J. Am. Chem. Soc.* **2004**, *126*, 1317.

(4) (a) Umezono, Y.; Fujita, W.; Awaga, K. *J. Am. Chem. Soc.* **2006**, *128*, 1084. (b) Jeannin, O.; Clerac, R.; Fourmigue, M. *J. Am. Chem. Soc.* **2006**, *128*, 14649. (c) Brefuel, N.; Shova, S.; Tuchagues, J. P. *Eur. J. Inorg. Chem.* **2007**, *27*, 4326.

(5) Cambi, L.; Gagnasso, A. *Atti. Accad. Naz. Lincei* **1931**, *13*, 809.

(6) (a) Cambi, L.; Szegö, L.; Cagnasso, A. *Atti. Accad. Naz. Lincei.* **1932**, *15*, 266. Cambi, L.; Szegö, L.; Cagnasso, A. (b) *Atti. Accad. Naz. Lincei.* **1932**, *15*, 329.

(7) Sorai, S.; Seki, S. *J. Phys. Chem. Solids* **1974**, *35*, 555.

(8) König, E.; Ritter, G.; Kulshreshtha, S. K. *Chem. Rev.* **1985**, *85*, 219.

(9) Fujita, W.; Awaga, K. *Science* **1999**, *286*, 261.

(10) Itkis, M. E.; Chi, X.; Cordes, A. W.; Haddon, R. C. *Science* **2002**, *296*, 1443.

(11) Miller, J. S. *Angew. Chem., Int. Ed.* **2003**, *42*, 27.

(12) (a) Leibeling, G.; Demeshko, S.; Dechert, S.; Meyer, F. *Angew. Chem., Int. Ed.* **2005**, *44*, 7111. (b) Demeshko, S.; Leibeling, G.; Dechert, S.; Meyer, F. *Dalton Trans.* **2006**, 3458. (c) Demeshko, S.; Leibeling, G.; Dechert, S.; Fuchs, S.; Pruschke, T.; Meyer, F. *ChemPhysChem* **2007**, *8*, 405.

(13) Demeshko, S.; Leibeling, G.; Maringgele, W.; Meyer, F.; Mennerich, C.; Klauss, H. H.; Pritzkow, H. *Inorg. Chem.* **2005**, *44*, 519.

(14) Ribas, J.; Escuer, A.; Monfort, M.; Vicente, R.; Cortés, R.; Lezama, L.; Rojo, T. *Coord. Chem. Rev.* **1999**, *193*−*195*, 1027.

(15) Ni, Z. P.; Ren, X. M.; Ma, J.; Xie, J. L.; Ni, C. L.; Chen, Z. D.; Meng, Q. J. *J. Am. Chem. Soc.* **2005**, *127*, 14330.

(16) Samir, Z.; Serguei, A. B. *J. Am. Chem. Soc.* **2005**, *127*, 16197.

(17) Heisenberg, W. Z. *Phys.* **1926**, *38*, 411.

(18) Kahn, O. *Molecular Magnetism*; VCH Publishers: New York, 1993.

(19) (a) Ruiz, E.; Cano, J.; Alvarez, S.; Alemany, P. *J. Comput. Chem.* **1999**, *20*, 1391. (b) Nagao, H.; Nishino, M.; Shigeta, Y.; Soda, T.; Kitagawa, Y.; Onishi, T.; Yoshioka, Y.; Yamaguchi, K. *Coord. Chem. Rev.* **2000**, *198*, 265. (c) Ciofini, I.; Dual, C. A. *Coord. Chem. Rev.* **2003**, *238*−*239*, 187. (d) Bencini, A.; Totti, F. *Int. J. Quantum Chem.* **2005**, *101*, 819. (e) Nunzi, F.; Ruiz, E.; Cano, J.; Alvarez, S. *J. Phys. Chem. C* **2007**, *111*, 618. (f) Koizumi, K.; Shoji, M.; Kitagawa, Y.; Takeda, R.; Yamanaka, S.; Kawakami, T.; Okumura, M.; Yamaguchi, K. *Polyhedron* **2007**, *26*, 2135.

(20) Ginsberg, A. P. *J. Am. Chem. Soc.* **1980**, *102*, 111.

(21) (a) Noodleman, L.; Norman, J. G., Jr. *J. Chem. Phys.* **1979**, *70*, 4903. (b) Noodleman, L. *J. Chem. Phys.* **1981**, *74*, 5737.

(22) Noodleman, L.; Davidson, E. R. *Chem. Phys.* **1986**, *109*, 131.

(23) Bencini, A.; Totti, F.; Daul, C. A.; Doclo, K.; Fantucci, P.; Barone, V. *Inorg. Chem.* **1997**, *36*, 5022.

(24) Ruiz, E.; Cano, J.; Alvarez, S.; Alemany, P. *J. Comput. Chem.* **1991**, *20*, 1391.

(25) Nagao, H.; Nishino, M.; Shigeta, Y.; Soda, T.; Kitagawa, Y.; Onishi, T.; Yoshioka, Y.; Yamaguchi, K. *Coord. Chem. Rev.* **2000**, *198*, 265.

(26) Onishi, T.; Soda, T.; Kitagawa, Y.; Takano, Y.; Daisuke, Y.; Takamizawa, S.; Yoshioka, Y.; Yamaguchi, K. *Mol. Cryst. Liq. Cryst.* **2000**, *343*, 133.

(27) Willett, R. W.; Willett, R. D.; Gatteschi, D.; Kahn, O. *Magneto-Structural Correlations in exchange Coupled Systems*; NATO Advanced Studies, Series C, Vol. 140; Reidel: Dordrecht, The Netherlands, 1983.

(28) Frisch, M. J.; et al. Gaussian 03, Gaussian, Inc.: Pittsburgh PA, 2003.

(29) Elnoor, A. A. N.; Zhang, J. P. *Chem. Phys.* **2006**, *330*, 82.

(30) Adamo, C.; Cossi, M.; Barone, V. *THEOCHEM* **1999**, *493*, 145.

(31) Hay, P. J.; Thibeault, J. C.; Hoffmann, R. *J. Am. Chem. Soc.* **1975**, *97*, 4884.

(32) Mitani, M.; Mori, H.; Takano, Y.; Yamaki, D.; Yoshioka, Y.; Yamaguchi, K. *J. Chem. Phys.* **2000**, *113*, 4035 and references therein.

(33) Kahn, O.; Sikorav, S.; Gouteron, J.; Jeannin, S.; Jeannin, Y. *Inorg. Chem.* **1983**, *22*, 2877.

(34) Aebersold, M. A.; Gillon, B.; Plantevin, O.; Pardi, L.; Kahn, O.; Bergerat, P.; Seggern, I. V.; Tuczek, F.; Öhrström, L.; Grand, A.; Lelièvre-Berna, E. *J. Am. Chem. Soc.* **1998**, *120*, 5238.